Chapter 4

Thin Plates

4.1 Introduction

In the previous two chapters, applications of T-elements to potential problems and elasto-statics were presented. Extension of the procedure to thin plate bending is described in this chapter. It should be noted that applications of the Trefftz method to plate bending have been the subject of fruitful scientific attention by many a distinguished researcher (e.g. Jin *et al.* [5], Jirousek [6], Qin [13], Venkatesh and Jirousek [17] and others). Jirousek and Leon [9] pioneered the application of T-elements to plate bending problems. Since then, various plate elements based on the hybrid-Trefftz approach have been presented, such as 9 DOF triangular elements [8] and an improved version [16], a family of 12 DOF quadrilateral elements [10], *h*- and *p*-elements [6]. Extensions of this procedure have been reported in [13] for thin plate on an elastic foundation, in [15] for transient plate bending analysis and in [14] for post-buckling analysis of thin plates. Alternatively, Jin *et al.* [5] developed a set of formulations, called Trefftz direct and indirect methods, for plate bending problems based on the weighted residual method. In this chapter, however, we will restrict our discussion to those results presented by [6,8,13].

4.2 Thin plate theory

A thin plate is a solid whose dimension is very small in one of the coordinate directions (direction x_3 in Fig. 4.1). When such a plate is subjected to both in-plane and transverse or normal loads as shown in Fig. 4.1, any point inside the plate can have displacement components *u*, *v* and *w* parallel to x_1, x_2 and x_3 axes respectively. In the linear theory of thin plates, the transverse deflection *w* is uncoupled from the in-plane displacements *u* and *v*. Consequently, the stiffness matrices for the in-plane and transverse deflections are also uncoupled and they can be calculated independently. Thus, if a plate is subjected to transverse loads and/or bending moments only, any point inside the plate experiences essentially a lateral displacement *w* (in-plane displacements *u* and *v* are also experienced because of the rotation of the plate element). In this case, the plate is said to be under the action of bending forces. In this section, the classical theory of thin plate bending is briefly reviewed.

In plate bending the plane $x_1 - x_2$ is taken to coincide with the mean surface of the plate (Fig. 4.2). The thickness of the plate is denoted by *t* (Fig. 4.2). The applied forces are per unit area inside the plate and per unit of length along the boundary Γ (Fig. 4.2). Forces can be given as direct forces or moments. The

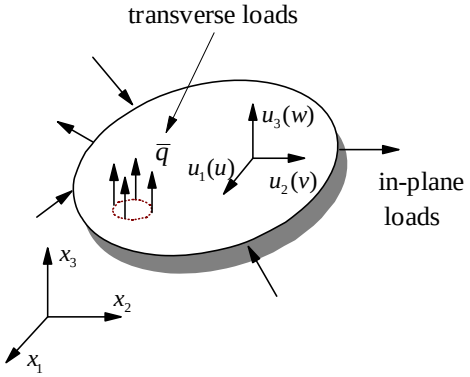

Fig. 4.1: Illustration of loads and displacements.

positive direction for moments and transverse shear forces is indicated in Fig. 4.2. The moments and shear forces are defined as

$$M_{11} = \int_{-t/2}^{t/2} \sigma_{11} x_3 dx_3 , \quad M_{22} = \int_{-t/2}^{t/2} \sigma_{22} x_3 dx_3 , \quad M_{12} = M_{21} = \int_{-t/2}^{t/2} \sigma_{12} x_3 dx_3 , \quad (4.1)$$

$$Q_1 = \int_{-t/2}^{t/2} \sigma_{13} dx_3 , \qquad Q_2 = \int_{-t/2}^{t/2} \sigma_{23} dx_3 . \quad (4.2)$$

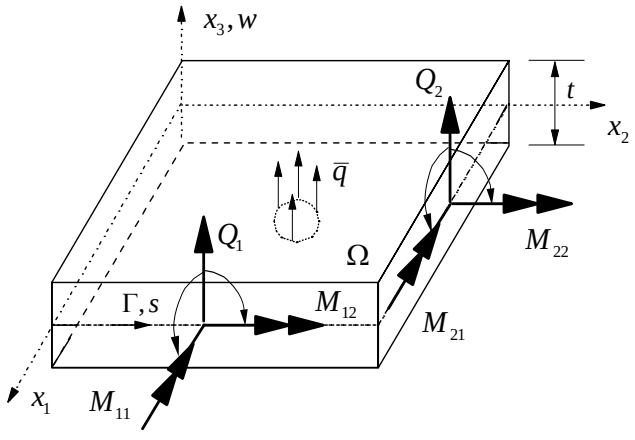

Fig. 4.2: Notation of moments and shear forces.

The equilibrium equations are given in terms of moments and shear forces as shown in Fig. 4.2, i.e.,

$$Q_{1,1} + Q_{2,2} + \bar{q} = 0, \quad M_{11,1} + M_{12,2} = Q_1, \quad M_{21,1} + M_{22,2} = Q_2, \tag{4.3}$$

where $\bar{q}$ is the distributed surface load. As the plate is thin in comparison to its length and width, any body force may be converted to an equivalent load $\bar{q}$ and hence no body force is considered separately in eqns (4.3).

If $n_i (i = 1,2)$ are cosines of the normal n with respect to x_i directions, we can write the boundary moments as

$$M_i = M_{ij} n_j, \tag{4.4}$$

where the boundary moments and rotations are shown in Fig. 4.3.

The natural way of writing the moments on the boundary is in terms of the resultant couples on the boundary (Fig. 4.3). This gives

$$M_n = M_1 n_1 + M_2 n_2 = M_{11} n_1^2 + 2M_{12} n_1 n_2 + M_{22} n_2^2, \tag{4.5}$$

$$M_{ns} = -M_1 n_2 + M_2 n_1 = -(M_{11} - M_{22}) n_1 n_2 + M_{12}(n_1^2 - n_2^2). \tag{4.6}$$

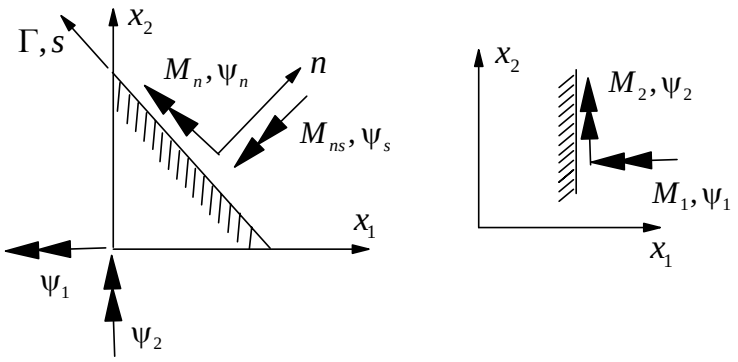

Fig. 4.3: Notation of boundary moments and rotations.

To derive the strain-displacement relations for a plate, consider the bending deformation of a small element (by neglecting shear deformation). Noting that in thin plate theory, the stresses σ_{11} (and σ_{22}, σ_{12}) and σ_{13} (and σ_{23}) are assumed to vary linearly and parabolically, respectively, over the thickness of the plate, and with the assumption of no in-plane deformation on the middle plane of the plate, the strains at any point in the element can be expressed as

$$\varepsilon_{11} = u_{1,1} = -z w_{,11}, \quad \varepsilon_{22} = u_{2,2} = -z w_{,22}, \tag{4.7a}$$

$$2\varepsilon_{12} = u_{1,2} + u_{2,1} = -2zw_{,12} \,. \tag{4.7b}$$

Equation (4.7) shows that the deflection *w*, which is a function of x_1 and x_2 only, completely describes the deformation state.

The moment-displacement relations can also be derived for thin plates. For this we assume the plate to be in a state of plane stress by considering the transverse stress σ_{33} to be negligibly small in comparison to in-plane stresses. Thus the stress-strain relations are given by eqn (1.59) together with eqn (1.68). By substituting eqn (4.7) into eqn (1.59) and then into eqns (4.1), we obtain after integration

$$M_{11} = -D(w_{,11} + \mu w_{,22}), \quad M_{22} = -D(w_{,22} + \mu w_{,11}),$$

$$M_{12} = -D(1-\mu)w_{,12} \,, \tag{4.8}$$

where *D* is defined in eqn (1.71). Equations (4.3) and (4.8) give

$$Q_1 = -D(w_{,11} + w_{,22})_{,1} \,, \quad Q_2 = -D(w_{,11} + w_{,22})_{,2} \,. \tag{4.9}$$

The boundary conditions of a thin plate are described as follows:

Essential boundary conditions:

$$w = \overline{w}, \quad \psi_n = \overline{\psi}_n \,, \quad \psi_s = \overline{\psi}_s \,, \qquad (\text{on } \Gamma_u), \tag{4.10}$$

where ψ_n and ψ_s are the rotation components tangential and normal to the boundary ($\psi_s = w_{,s}$ and $\psi_n = w_{,n}$).

Natural boundary conditions:

$$Q_n = Q_i n_i = \overline{Q}_n \,, \quad M_n = \overline{M}_n \,, \quad M_{ns} = \overline{M}_{ns} \,, \qquad (\text{on } \Gamma_\sigma), \tag{4.11}$$

where *n* and *s* are the outward normal and the tangent to the plate boundary, and $(\,)_{,n} = (\,)_{,i} n_i$, $(\,)_{,s} = (\,)_{,i} s_i$.

In Kirchhoff plate theory, one may specify only two among the above three pairs of boundary conditions. This problem may be circumvented by introducing a new variable, equivalent shear force *R*, in such a way that

$$R = M_{ij,j} n_i + M_{ns,s} \,. \tag{4.12}$$

Using this new variable the boundary conditions can now be given as

$$w = \overline{w} \,, \qquad (\text{on } \Gamma_w), \tag{4.13}$$

$$w_{,n} = w_{,i} n_i = \overline{w}_{,n} \,, \qquad (\text{on } \Gamma_{w_n}), \tag{4.14}$$

$$R = \overline{R} \,, \qquad (\text{on } \Gamma_R), \tag{4.15}$$

$$M_n = \overline{M}_n, \qquad (\text{on } \Gamma_{M_n}), \tag{4.16}$$

where $\Gamma = \Gamma_w + \Gamma_R = \Gamma_{w_n} + \Gamma_{M_n}$.

In the classical theory of thin plates, first the deflection *w* is found by solving the equilibrium equations (4.3) under the prescribed loading condition $\overline{q}$. By substituting eqn (4.9) into eqn (4.3), one obtains

$$D\left(\frac{\partial^4 w}{\partial x_1^4} + 2\frac{\partial^4 w}{\partial x_1^2 \partial x_2^2} + \frac{\partial^4 w}{\partial x_2^4}\right) = \overline{q}\,. \tag{4.17}$$

Thus the problem is to solve the fourth order partial differential equation (4.17) by using appropriate boundary conditions. Once *w* is found, the strains, stresses and moments developed in the plate can be determined by using eqns (4.7), (1.59) and (4.8) respectively. It should be mentioned that the closed form solution of eqn (4.17) cannot be obtained except for plates having a simple configuration (like rectangular and circular plates) as well as simple loading and boundary conditions. However, numerical methods, such as the T-element approach, can be used for analyzing problems involving plates of arbitrary planeform and loading conditions which might, sometimes, have singular corners or cracks. The corresponding T-element approach is described in the following sections of this chapter.

4.3 Assumed field

The internal displacement field in a thin plate element is assumed as

$$w = \breve{w} + \sum_{j=1}^{m} N_j c_j = \breve{w} + \mathbf{N}\mathbf{c}\,, \tag{4.18}$$

where c_j are undetermined coefficients, and $\breve{w}$ and N_j are known functions which should be chosen so that

$$D\nabla^4 \breve{w} = \overline{q} \quad \text{and} \quad \nabla^4 N_j = 0\,, \qquad (j = 1,2,\cdots,m)\,, \tag{4.19}$$

everywhere in the element sub-domain Ω_e, where $\nabla^4 = \partial^4/\partial x_1^4 + 2\partial^4/\partial x_1^2 \partial x_2^2 + \partial^4/\partial x_2^4$ is the biharmonic operator. From eqns (4.5) and (4.12)-(4.14), the generalized boundary forces and displacements are readily derived and denote

$$R = M_{ij,j} n_i + M_{ns,s} = \mathbf{W}_1 \mathbf{c} + \breve{R}\,, \tag{4.20}$$

$$M_n = M_{ij} n_i n_j = \mathbf{W}_2 \mathbf{c} + \breve{M}_n\,, \tag{4.21}$$

$$w_{,n} = w_{,i} n_i = \mathbf{W}_3 \mathbf{c} + \breve{w}_{,n}\,, \tag{4.22}$$

where $\breve{R}, \breve{M}_n, \breve{w}_{,n}$ and $\mathbf{W}_i (i = 1,2,3)$ correspond respectively to the particular and homogeneous parts. For example,

$$\breve{M}_n = \breve{M}_{ij} n_i n_j = -D[(1-\mu)\breve{w}_{,ij} + \mu \delta_{ij} \breve{w}_{,kk}] n_i n_j \,. \tag{4.23}$$

In the hybrid approach under consideration, the elements are linked through an auxiliary displacement frame

$$\tilde{\mathbf{v}} = \begin{Bmatrix} \tilde{w} \\ \tilde{w}_{,n} \end{Bmatrix} = \begin{bmatrix} \tilde{\mathbf{N}}_1 \\ \tilde{\mathbf{N}}_2 \end{bmatrix} \mathbf{d} = \tilde{\mathbf{N}} \mathbf{d} \,, \tag{4.24}$$

where $\mathbf{d}$ stands for the vector of nodal parameters and $\tilde{\mathbf{N}}$ is the conventional finite element interpolating matrix such that the corresponding nodal parameters of the adjacent elements are matched, $\tilde{\mathbf{v}}$ is the same for the two elements over their common boundary.

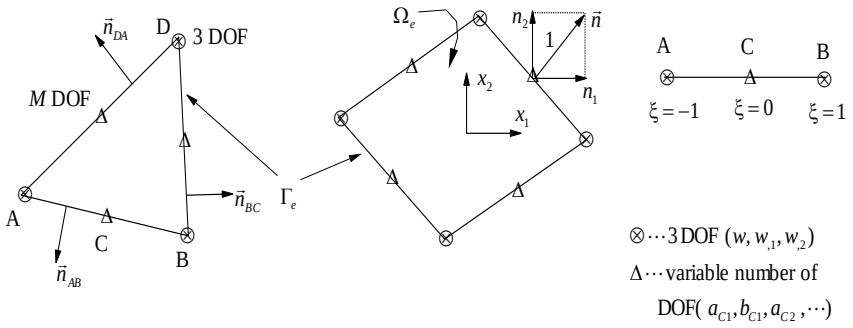

Fig. 4.4: Hybrid-Trefftz plate bending element.

As an illustration, consider the side A-B of a particular element (Fig. 4.4). A simple interpolation of the frame displacements can be given in the form [13]

$$(\tilde{w})_{AB} = \tilde{N}_3 w_A + \frac{1}{2}(w_{2A} n_1 - w_{1A} n_2) l_{AB} \tilde{N}_4$$

$$+ \tilde{N}_5 w_B + \frac{1}{2}(w_{2B} n_1 - w_{1B} n_2) l_{AB} \tilde{N}_6 = \tilde{\mathbf{N}}_{AB1} \mathbf{d}_{AB} \,, \tag{4.25}$$

$$(\tilde{w}_{,n})_{AB} = w_{iA} n_i \tilde{N}_1 + w_{iB} n_i \tilde{N}_2 = \tilde{\mathbf{N}}_{AB2} \mathbf{d}_{AB} \,, \tag{4.26}$$

where $w_{iA} = (\partial w / \partial x_i)\big|_A$, $w_{iB} = (\partial w / \partial x_i)\big|_B$, l_{AB} is the length of side AB, $\tilde{N}_1$ and $\tilde{N}_2$ are defined in eqn (2.27), and $\tilde{N}_i$ (i=3-6) are shape functions defined by

$$\tilde{N}_3 = \frac{1}{4}(\xi^3 - 3\xi + 2), \quad \tilde{N}_4 = \frac{1}{4}(\xi^3 - \xi^2 - \xi + 1),$$
$$\tilde{N}_5 = -\frac{1}{4}(\xi^3 - 3\xi - 2), \quad \tilde{N}_6 = \frac{1}{4}(\xi^3 + \xi^2 - \xi - 1), \tag{4.27}$$

and where $\mathbf{d}_{AB} = \{w_A, w_{1A}, w_{2A}, w_B, w_{1B}, w_{2B}\}^T$.

4.4 T-complete functions and particular solutions

4.4.1 T-complete solution

Based on the approach of variable separation, the T-complete solution of the biharmonic equation (4.17) can be found [4,5]:

$$w = \sum_{n=0}^{\infty} \{\mathrm{Re}[(a_n + r^2 b_n) z^n] + \mathrm{Im}[(c_n + r^2 d_n) z^n]\}, \tag{4.28}$$

where

$$r^2 = x_1^2 + x_2^2, \quad z = x_1 + i x_2 . \tag{4.29}$$

Hence, the T-complete system of solutions for plate bending problems can be taken as

$$\mathrm{T} = \{1, r^2, \mathrm{Re}\, z^2, \mathrm{Im}\, z^2, r^2\, \mathrm{Re}\, z, r^2\, \mathrm{Im}\, z, \mathrm{Re}\, z^3, \cdots\} . \tag{4.30}$$

Example 4.1: Give the explicit expressions of matrices **N** in eqn (4.18), $\tilde{\mathbf{N}}$ in eqn (4.24) and the vector of nodal parameters **d** for a typical HT-triangular plate bending element as shown in Fig. 4.4.

As suggested by Jirousek [7], the matrix **N** for the 9 DOF triangular plate element may be formed by seven functions chosen from system (4.30) as

$$\mathbf{N} = \{r^2, x_1^2 - x_2^2, 2x_1x_2, x_1 r^2, x_2 r^2, x_1^3 - 3x_1 x_2^2, 3x_1^2 x_2 - x_2^3\} . \tag{4.31}$$

Obviously this choice satisfies the rank condition (2.51) as

$$m = 7 \geq k - r = 9 - 3 = 6 . \tag{4.32}$$

Note that truncation of the series (4.30) should occur such that the solution would be direction-insensitive. In order to fulfill this condition, *m* has been increased to 7, to contain all linearly independent biharmonic polynomials of the 2nd and 3rd degree.

Using the notation shown in Fig. 4.4, the vector **d** can be expressed as

$$\mathbf{d} = \{w_A, w_{1A}, w_{2A}, w_B, w_{1B}, w_{2B}, w_D, w_{1D}, w_{2D}\}^T , \tag{4.33}$$

and then the corresponding matrix $\tilde{\mathbf{N}}$ can be obtained by using the function

β_{ij} defined in eqn (2.28) as

$$\tilde{\tilde{\mathbf{N}}} = \begin{bmatrix} \tilde{\tilde{N}}_a(AB,DA) & \tilde{\tilde{N}}_b(AB,DA) & \tilde{\tilde{N}}_c(AB,DA) & \tilde{\tilde{N}}_a(BD,AB) & \tilde{\tilde{N}}_b(BD,AB) \\ 0 & \tilde{\tilde{N}}_d(AB,DA) & \tilde{\tilde{N}}_e(AB,DA) & 0 & \tilde{\tilde{N}}_d(BD,AB) \end{bmatrix}$$

$$\begin{bmatrix} \tilde{\tilde{N}}_c(BD,AB) & \tilde{\tilde{N}}_a(DA,BD) & \tilde{\tilde{N}}_b(DA,BD) & \tilde{\tilde{N}}_c(DA,BD) \\ \tilde{\tilde{N}}_e(BD,AB) & 0 & \tilde{\tilde{N}}_d(DA,BD) & \tilde{\tilde{N}}_e(DA,BD) \end{bmatrix}, \tag{4.34}$$

where

$$\tilde{\tilde{N}}_a(p,q) = \tilde{\tilde{N}}_3\beta_p + \tilde{\tilde{N}}_5\beta_q\,, \tag{4.35}$$

$$\tilde{\tilde{N}}_b(p,q) = -\frac{n_{p2}l_p}{2}\tilde{\tilde{N}}_4\beta_p - \frac{n_{q2}l_q}{2}\tilde{\tilde{N}}_6\beta_q\,, \tag{4.36}$$

$$\tilde{\tilde{N}}_c(p,q) = \frac{n_{p1}l_p}{2}\tilde{\tilde{N}}_4\beta_p + \frac{n_{q1}l_q}{2}\tilde{\tilde{N}}_6\beta_q\,, \tag{4.37}$$

$$\tilde{\tilde{N}}_d(p,q) = n_{p1}\tilde{\tilde{N}}_1\beta_p + n_{q1}\tilde{\tilde{N}}_2\beta_q\,, \tag{4.38}$$

$$\tilde{\tilde{N}}_e(p,q) = n_{p2}\tilde{\tilde{N}}_1\beta_p + n_{q2}\tilde{\tilde{N}}_2\beta_q\,, \tag{4.39}$$

and $n_p(=n_{AB},n_{BD},n_{DA})$ as shown in Fig. 4.4.

4.4.2 Particular solution

The particular solution $\breve{w}$ in eqn (4.18) can be derived by way of its source (or Green's) function, which represents the field generated by a concentrated unit point force. For a thin isotropic plate the source function of the governing equation

$$D\nabla^4 w^* = \delta(P,Q)\,, \tag{4.40}$$

where $\delta(P,Q)$ is the Dirac delta function, point 'P' and 'Q' are defined in Section 2.4, is given by [3]

$$w^*(r_{PQ}) = \frac{r_{PQ}^2}{8\pi D}\ln r_{PQ}\,, \tag{4.41}$$

where r_{PQ} is defined in Section 2.4.

Using this source function the particular solution $\breve{w}$ in eqn (4.18) can be expressed as

$$\breve{w}(P) = \int_{\Omega} \overline{q}(Q) w^*(r_{PQ}) d\Omega(Q) . \tag{4.42}$$

For some special loading conditions, the particular solution can be obtained analytically. Suitable expressions for uniform load $\overline{q}$ and concentrated load $\overline{P}$ (applied at x_{1Q}, x_{2Q}) are, for example,

$$\breve{w} = \frac{\overline{q}(x_1^2 + x_2^2)^2}{64D} \quad \text{and} \quad \breve{w} = \frac{\overline{P}}{8\pi D} r_{PQ}^2 \ln r_{PQ} . \tag{4.43}$$

The drawback of the latter expression, representing the well-known elasticity solution of an infinite plate, is the fact that the solution is irrelevant in the vicinity of $\overline{P}$. Indeed, for $x_{1P} \to x_{1Q}$, $x_{2P} \to x_{2Q}$, the deformations and consequently the moments in the plate tend to infinity and consequently violate the assumption of small deformation of linear elasticity. In practice, a concentrated load is distributed over a small portion of the plate and the engineer is interested in the corresponding peak values of moments. A more realistic approach is therefore to assume that $\overline{P}$ is distributed uniformly over a small circular area of optional rayon *b* (Fig. 4.5). Solving the infinite plate problem again yields

$$\breve{w} = \left[\frac{\beta^2}{64}(4\ln\beta - 3) + \frac{1}{16} + \frac{\rho^2}{32}(4\ln\beta - \beta^2) + \frac{\rho^4}{64\beta^2} \right] \frac{\overline{P} a^2}{\pi D}, \quad (\text{for } \rho \le \beta), \tag{4.44}$$

$$\breve{w} = \left[\frac{1}{32}(2 + \beta^2)(1 - \rho^2) + \frac{1}{16}(\beta^2 + 2\rho^2)\ln\rho \right] \frac{\overline{P} a^2}{\pi D}, \quad (\text{for } \rho \ge \beta). \tag{4.45}$$

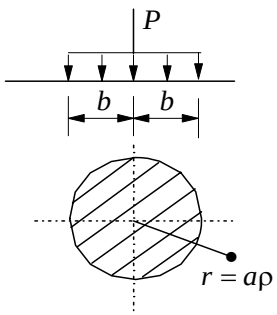

$a > 0 \cdots$ optional constant

$\rho = r/a; \quad \beta = b/a$

Fig. 4.5: Representation of concentrated loads.

4.5 Variational formulations for plate bending

The T-element formulation for thin plate bending can be derived by means of the modified variational principle [13]. The related functional used for deriving the

hybrid Trefftz element formulation is constructed as

$$\Pi_m = \sum_e \{\Pi_e - \int_{\Gamma_{e2}} (\overline{M}_n - M_n) w_{,n} ds + \int_{\Gamma_{e4}} (\overline{R} - R) w ds + \int_{\Gamma_{e5}} (M_n \tilde{w}_{,n} - R\tilde{w}) ds\}, \tag{4.46}$$

where

$$\Pi_e = \int_{\Omega_e} U d\Omega + \int_{\Gamma_{e1}} M_n \overline{w}_{,n} ds - \int_{\Gamma_{e3}} R\overline{w} ds, \tag{4.47}$$

with

$$U = \frac{1}{2D(1-\mu^2)}[(M_{11} + M_{22})^2 + 2(1+\mu)(M_{12}^2 - M_{11}M_{22})], \tag{4.48}$$

and where eqn (4.17) is assumed to be satisfied, *a priori*. The boundary Γ_e of a particular element consists of the following parts:

$$\Gamma_e = \Gamma_{e1} + \Gamma_{e2} + \Gamma_{e5} = \Gamma_{e3} + \Gamma_{e4} + \Gamma_{e5}, \tag{4.49}$$

where

$$\Gamma_{e1} = \Gamma_e \cap \Gamma_{w_n},\ \Gamma_{e2} = \Gamma_e \cap \Gamma_M,\ \Gamma_{e3} = \Gamma_e \cap \Gamma_w,\ \Gamma_{e4} = \Gamma_e \cap \Gamma_R, \tag{4.50}$$

and Γ_{e5} is the inter-element boundary of the element.

The stationary property of the functional (4.46) can be easily obtained by taking its variation and noting that eqn (4.17) holds, *a priori*, by the previous assumption. The result is as follows:

$$\begin{aligned}\delta\Pi_m = &-\int_{\Gamma_{w_n}} (w_{,n} - \overline{w}_{,n}) \delta M_n ds + \int_{\Gamma_w} (w - \overline{w}) \delta R ds \\ &+ \int_{\Gamma_M} (M_n - \overline{M}_n) \delta w_{,n} ds - \int_{\Gamma_R} (R - \overline{R}) \delta w ds \\ &+ \sum_e \int_{\Gamma_{e5}} [(\tilde{w}_{,n} - w_{,n}) \delta M_n - (\tilde{w} - w) \delta R + M_n \delta \tilde{w}_{,n} - R\delta\tilde{w}] ds.\end{aligned} \tag{4.51}$$

Hence, the Euler equations for eqn (4.51) are the boundary conditions (4.13)-(4.16) and

$$w_e = w_f,\ \ R_e = -R_f,\ \ w_{,ne} = -w_{,nf},\ \ M_{ne} = M_{nf},\ \ (\text{on } \Gamma_e \cap \Gamma_f), \tag{4.52}$$

where '*e*' and '*f* ' stand for any two neighboring elements and the subscripts '*ne*' and '*nf* ' represent the outward normal directions to the boundary of elements *e* and *f*, respectively.

Consequently, the stationary condition of eqn (4.51) implicitly imposes all the missing conditions and, as such, constitutes a suitable basis for a T-element formulation.

4.6 Generation of element stiffness matrix

The element stiffness matrix may be established by setting $\delta\Pi_{me} = 0$. To simplify the calculation of the element matrix, we first transform the domain integral in eqn (4.46) into boundary integral. In fact, by reason of solution properties of the intra-element trial functions and using the Gauss divergence theorem, the functional Π_{me} can be simplified to

$$\begin{aligned}\Pi_{me} = &\frac{1}{2}\int_{\Omega_e} \bar{q} w d\Omega + \int_{\Gamma_{e1}} M_n \overline{w}_{,n} ds - \int_{\Gamma_{e3}} R\overline{w} ds \\ &+ \int_{\Gamma_{e2}} (M_n - \overline{M}_n) w_{,n} ds - \int_{\Gamma_{e4}} (R - \overline{R}) w ds \\ &+ \frac{1}{2}\int_{\Gamma_e} (Rw - M_n w_{,n}) ds - \int_{\Gamma_{e5}} (R\tilde{w} - M_n \tilde{w}_{,n}) ds.\end{aligned} \tag{4.53}$$

Substitution of eqns (4.18), (4.20)-(4.22) and (4.24) into eqn (4.53) yields

$$\Pi_{me} = -\frac{1}{2}\mathbf{c}^T\mathbf{H}\mathbf{c} + \mathbf{c}^T\mathbf{S}\mathbf{d} + \mathbf{c}^T\mathbf{r}_1 + \mathbf{d}^T\mathbf{r}_2 + \text{terms without } \mathbf{c} \text{ or } \mathbf{d}, \tag{4.54}$$

where the matrices **H**, **S** and vectors $\mathbf{r}_1$, $\mathbf{r}_2$ are

$$\mathbf{H} = \int_{\Gamma_e} (\mathbf{W}_2^T\mathbf{W}_3 - \mathbf{N}^T\mathbf{W}_1) ds - \int_{\Gamma_{e2}} \mathbf{W}_2^T\mathbf{W}_3 ds + \int_{\Gamma_{e4}} \mathbf{N}^T\mathbf{W}_1 ds\,, \tag{4.55}$$

$$\mathbf{S} = \int_{\Gamma_{e5}} (\mathbf{W}_2^T\tilde{\mathbf{N}}_2 - \mathbf{W}_1^T\tilde{\mathbf{N}}_1) ds\,, \tag{4.56}$$

$$\begin{aligned}\mathbf{r}_1 = &\frac{1}{2}\int_{\Omega_e} \mathbf{N}^T\bar{q} d\Omega + \frac{1}{2}\int_{\Gamma_e} (\mathbf{W}_1^T\breve{w} + \mathbf{N}^T\breve{R} - \mathbf{W}_2^T\breve{w}_{,n} - \mathbf{W}_3^T\breve{M}_n) ds \\ &+ \int_{\Gamma_{e2}} \mathbf{W}_2^T\breve{w}_{,n} ds - \int_{\Gamma_{e4}} \mathbf{W}_1^T\breve{w} ds + \int_{\Gamma_{e1}} \mathbf{W}_2^T\overline{w}_{,n} ds - \int_{\Gamma_{e3}} \mathbf{W}_1^T\overline{w} ds,\end{aligned} \tag{4.57}$$

$$\mathbf{r}_2 = \int_{\Gamma_{e5}} (\tilde{\mathbf{N}}_2^T\breve{M}_n - \tilde{\mathbf{N}}_1^T\breve{R}) ds\,, \tag{4.58}$$

in which $\tilde{\mathbf{N}}_1, \tilde{\mathbf{N}}_2$ are defined in eqn (4.24) and their expressions typical to a 9 DOF triangular element have been given in eqn (4.34), and **N** is also given in eqn (4.31) for a 9 DOF triangular element. From eqns (4.20)-(4.22), $\mathbf{W}_i$ (i=1-3) can be expressed in terms of **N** explicitly as

$$\mathbf{W}_1 = -D[(1-\mu)(\mathbf{N}_{,ijj}n_i + \mathbf{N}_{,ijs}n_i s_j) + \mu\delta_{ij}(\mathbf{N}_{,jkk}n_i + \mathbf{N}_{,kks}n_i s_j)], \tag{4.59}$$

$$\mathbf{W}_2 = -D[(1-\mu)\mathbf{N}_{,ij} + \mu\delta_{ij}\mathbf{N}_{,kk})]n_i n_j, \tag{4.60}$$

$$\mathbf{W}_3 = \mathbf{N}_{,i}n_i. \tag{4.61}$$

Similarly, $\breve{M}_n$, $\breve{R}$ and $\tilde{\breve{w}}_{,n}$ can be expressed in terms of $\breve{w}$ by using eqns (4.20)-(4.22). Thus the main task of next step is to evaluate the particular solution $\breve{w}$. $\breve{w}$ has different form for different loading conditions, which has been discussed in Section 4.4 and will be further addressed in Section 4.8.

As was done before, the vector of undetermined parameters **c** may be eliminated at the element level by relating it to the nodal parameters **d**:

$$\mathbf{c} = \mathbf{H}^{-1}(\mathbf{S}\mathbf{d} + \mathbf{r}_1). \tag{4.62}$$

Substituting eqn (4.62) into eqn (4.54) yields the expression of Π_{me} in terms of **d** only, in the form

$$\Pi_{me} = -\tfrac{1}{2}\mathbf{d}^T\mathbf{S}^T\mathbf{H}^{-1}\mathbf{S}\mathbf{d} + \mathbf{d}^T(\mathbf{S}^T\mathbf{H}^{-1}\mathbf{r}_1 + \mathbf{r}_2). \tag{4.63}$$

The vanishing variation of Π_{me} with respect to **d** leads to the following force-displacement relationship for T-element formulation:

$$\mathbf{K}\mathbf{d} = \mathbf{P}, \tag{4.64}$$

where $\mathbf{K} = \mathbf{S}^T\mathbf{H}^{-1}\mathbf{S}$ is the stiffness matrix for the T-element approach and **P**= $\mathbf{S}^T\mathbf{H}^{-1}\mathbf{r}_1$ the equivalent nodal force vector.

It should be pointed out that the trial functions being defined and the nature of the approach (no integration involved over the element area) make it possible to write a subroutine for a very general polygonal element with optional frame functions and a variable number of sides. This enables a variety of elements, from the very simple to the most sophisticated, to be generated. Typical examples of triangular and quadrilateral elements are shown in Fig. 4.4.

For the reason explained in Section 3.6, the trial functions (4.18) do not include the rigid body motion modes (1, *x* and *y*). Thus, once the element assembly has been solved for nodal parameters, the displacement may be calculated anywhere at the element boundary (the frame function $\tilde{w}$) but not inside the element. While this may be of no concern for the simplest triangular element, knowledge of displacement at interior points becomes increasingly important as element accuracy augments. Therefore, it is of interest now to complete the lacking rigid body motion terms and write the interior displacement field of a particular element as

$$w = \breve{w} + \mathbf{N}\mathbf{c} + \{1 \;\; x \;\; y\}\mathbf{c}_r, \tag{4.65}$$

where the vector **c** may now be considered as known. The undetermined rigid body motion parameters $\mathbf{c}_r$ may then be calculated, for example, from the least square matching of w and $\tilde{w}$ at the corner nodes of the element:

$$\sum_{j=1}^{N}(w_j - \tilde{w}_j)^2 = \min , \tag{4.66}$$

where N is the number of nodes for the element. Equation (4.66) provides

$$\mathbf{c}_r = -\mathbf{H}_r^{-1}\mathbf{h}_r , \tag{4.67}$$

with

$$\mathbf{H}_r = \sum_{i=1}^{N}\begin{bmatrix} 1 & x_{1i} & x_{2i} \\ x_{1i} & x_{1i}^2 & x_{1i}x_{2i} \\ x_{2i} & x_{1i}x_{2i} & x_{2i}^2 \end{bmatrix}, \quad \mathbf{h}_r = \sum_{i=1}^{N}(\breve{w} + \mathbf{N}\mathbf{c} - \tilde{w})_i \begin{Bmatrix} 1 \\ x_{1i} \\ x_{2i} \end{Bmatrix}. \tag{4.68}$$

4.7 *p*-method elements

The HT thin plate *p*-elements constructed below are made of the internal displacement field (eqn (4.18)) and a single type of displacement frame, involving 3 DOF (one deflection and two rotation components) at corner nodes and an optional number of hierarchical side mode DOF associated with mid-side nodes (Fig. 4.4). In this case, all formulations described above remain unchanged except the frame field (4.24). A typical HT *p*-element is shown in Fig. 4.4, in which amplitudes are $a_{C1}, a_{C2}\cdots$ for deflection $\tilde{w}$, $b_{C1}, b_{C2}\cdots$ for normal slope $\tilde{w}_{,n}$. As an illustration, consider the side A-C-B of a particular element (Fig. 4.4). The frame functions are defined as an extension of eqns (4.25) and (4.26) in the form

$$\begin{aligned}(\tilde{w})_{AB} = {} & \tilde{N}_3 w_A + \tfrac{1}{2}(w_{2A}n_1 - w_{1A}n_2)l_{AB}\tilde{N}_4 \\ & + \tilde{N}_5 w_B + \tfrac{1}{2}(w_{2B}n_1 - w_{1B}n_2)l_{AB}\tilde{N}_6 + \sum_{J=1}^{M} L_J a_{CJ} ,\end{aligned} \tag{4.69}$$

$$(\tilde{w}_{,n})_{AB} = w_{iA}n_i\tilde{N}_1 + w_{iB}n_i\tilde{N}_2 + \sum_{J=1}^{M} M_J b_{CJ} , \tag{4.70}$$

where

$$L_J = \xi^{J-1}(1-\xi^2)^2, \qquad M_J = \xi^{J-1}(1-\xi^2) . \tag{4.71}$$

Using such elements enables one to maintain not only the finite element grid but

also the number of nodes fixed while preserving the possibility of controlling the solution accuracy by simply acting simultaneously on the number M of DOF associated with mid-side nodes (M may be different for each mid-node) and the number m of trial functions N_j. Thus the initial definition of the FE-grid remains unchanged during the whole process. The additional advantage is that the FE-equations will have a more dominantly diagonal form due to the use of the relative variables a_{Ci}, b_{Ci} and as a consequence will exhibit improved conditioning, resulting in a lower truncation error. Moreover, such variables do not lead to undue 'overcompatibility' as would the use, for example, of additional higher order DOF at corner nodes.

4.8 Special purpose functions

In this section, we present some special purpose functions, which offer a very accurate analysis of stress concentrations attributable to discontinuous loads or local geometry defects through the use of special homogeneous solutions N_j and/or a suitable particular solution $\breve{w}$. We deal with line load [17], singular corner [8], and circular holes [8].

4.8.1 Line load

In this case all formulations given in the previous sections remain unchanged except the particular solution $\breve{w}$. The particular solution $\breve{w}$ for a uniformly distributed line load (Fig. 4.6) can be obtained by integrating the expressions in eqn (4.43) along the segment AB, leading to

$$\breve{w} = \frac{pd^3}{16\pi D}\left[\left(\chi + \frac{\chi^3}{3}\right)\left(\ln\frac{d^2(1+\chi^2)}{a^2} - \frac{2}{3}\right) - \frac{2\chi}{3} + \frac{4}{3}\arctan\chi\right]_{\theta_A}^{\theta_B}, \qquad (4.72)$$

for the case of Fig. 4.6(a), and

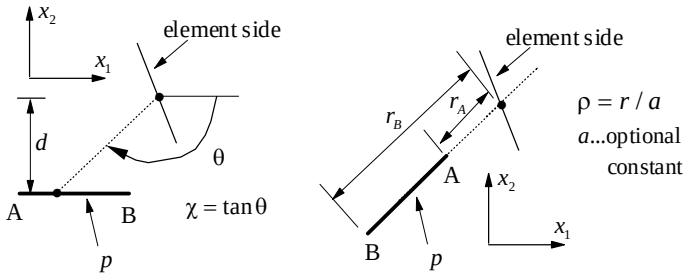

(a) (b)

Fig. 4.6: Line load. (a) arbitrarily located, (b) in line with integrated point.

$$\breve{w} = \frac{pa^3\rho^3}{144\pi D}(2 - 6\ln\rho)\Big|_{\rho_A}^{\rho_B}, \tag{4.73}$$

for the case of Fig. 4.6(b), where χ and ρ are defined in Fig. 4.6.

4.8.2 Singular corner

The singular corner to be considered is shown in Fig. 2.7, showing an infinite wedge with particular boundary conditions along the sides $\theta = \pm\theta_0$. Then, writing the governing plate equation in polar coordinates (r, θ),

$$D\left(\frac{\partial^2}{\partial r^2} + \frac{\partial}{r\partial r} + \frac{\partial^2}{r^2\partial\theta^2}\right)^2 w = \overline{q}, \tag{4.74}$$

enables *w* to be assumed in the form

$$w = \breve{w} + r^{\lambda+1}F(\theta, \lambda). \tag{4.75}$$

Substituting eqn (4.75) into eqn (4.74), the homogeneous part of the solution is

$$\begin{aligned} F(\theta,\lambda) = {} & C_1\sin(\lambda+1)\theta + C_2\cos(\lambda+1)\theta \\ & + C_3\sin(\lambda-1)\theta + C_4\cos(\lambda-1)\theta, \end{aligned} \tag{4.76}$$

where C_1 to C_4 are constants to be determined from boundary conditions at $\theta = \pm\theta_0$. Since the system of the four simultaneous equations representing these conditions is homogeneous, the solution leads to a transcendental equation for λ and the corresponding eigenfunctions $F(\theta,\lambda)$, which may be found for various boundary conditions [18]. For example, the solution for a simply supported obtuse corner ($2\theta_0 < \pi$) is as follows

$$N_{j+1} = r^{\lambda+1}\cos(\lambda-1)\theta, \quad \lambda = \frac{1}{\theta_0}\left(\frac{\pi}{2} + \theta_0 + k\pi\right), \quad k = 0,1,2\cdots, \tag{4.77}$$

$$N_{j+2} = r^{\lambda+1}\cos(\lambda+1)\theta, \quad \lambda = \frac{1}{\theta_0}\left(\frac{\pi}{2} - \theta_0 + k\pi\right), \quad k = 0,1,2\cdots, \tag{4.78}$$

$$N_{j+3} = r^{\lambda+1}\sin(\lambda-1)\theta, \quad \lambda = \frac{k\pi}{\theta_0} + 1, \quad k = 1,2\cdots, \tag{4.79}$$

$$N_{j+3} = r^{\lambda+1}\sin(\lambda+1)\theta, \quad \lambda = \frac{k\pi}{\theta_0} - 1, \quad k = 1,2\cdots. \tag{4.80}$$

It should be noted that the use of eqns (4.65)-(4.68) is not required for such

elements, as the kinematic conditions fulfilled by these functions at the element boundaries $\theta = \pm\theta_0$ prevent the appearance of rigid body motion modes.

The next step is to find a suitable particular solution $\breve{w}$ for a given load and boundary conditions. For uniform load $\bar{q}$, for example, a solution may be obtained by completing the particular integral (4.43), which does not fulfill any boundary conditions, by appropriate corrective terms to restore the prescribed conditions at $\theta = \pm\theta_0$. Taking this into account, the particular solution $\breve{w}$ for a simply-supported obtuse corner ($2\theta_0 < \pi$) is as follows:

(a) $\cos 4\theta_0 \neq 0, \quad \cos 2\theta_0 \neq 0 \quad (\theta_0 \neq \pi/8, \pi/4, 3\pi/8)$

$$\breve{w} = \frac{\bar{q}a^4\rho^4}{64D}\left(1 + \frac{\cos 4\theta}{3\cos 4\theta_0} - \frac{4\cos 2\theta}{3\cos 2\theta_0}\right). \tag{4.81}$$

(b) $(\theta_0 = \pi/8,\ 3\pi/8)$

$$\breve{w} = \frac{\bar{q}a^4\rho^4}{64D}\left(1 + \frac{\theta \sin 4\theta}{3\theta_0 \sin 4\theta_0} - \frac{4\cos 2\theta}{3\cos 2\theta_0} - \ln\rho \frac{\cos 4\theta}{3\theta_0 \sin 4\theta_0}\right). \tag{4.82}$$

(c) $\cos 2\theta_0 = 0 \qquad (\theta_0 = \pi/4)$

$$\breve{w} = \frac{\bar{q}a^4\rho^4}{64D}\left(1 + \frac{\cos 4\theta}{3\cos 4\theta_0} - \frac{4\theta\cos 2\theta}{3\theta_0 \cos 2\theta_0} + \ln\rho \frac{4\cos 2\theta}{3\theta_0 \sin 2\theta_0}\right). \tag{4.83}$$

4.8.3 Circular hole

Appropriate special purpose functions for a perforated element are found by considering an infinite perforated plate (Fig. 2.7) for which the solution to eqn (4.74) may be assumed in the form

$$w = \breve{w} + \sum_k [F_k(r)\sin k\theta + G_k(r)\cos k\theta], \quad (k = 0,1,2\cdots). \tag{4.84}$$

Substituting eqn (4.84) into (4.74) leads to

$$F_k(r) = \sum_{j=1}^{4} A_{kj} f_{kj}(r), \qquad G_k(r) = \sum_{j=1}^{4} B_{kj} g_{kj}(r), \tag{4.85}$$

where $f_{kj}(r), g_{kj}(r)$ are the known fundamental solution functions and A_{kj}, B_{kj} are undetermined constants, half of which may be eliminated by fulfilling (for any k separately for the terms associated with $\sin k\theta$ and $\cos k\theta$) the homogeneous

boundary conditions at the hole boundary $r=b$. The remaining constants become the undetermined coefficients c_i of the element expansion set. For a circular hole with free boundary conditions, the trial functions N_j are given by [8]:

$$N_1 = \ln\rho + \frac{1-\mu}{2(1+\mu)}\rho^2 , \tag{4.86}$$

$$N_2 = (\rho^3 - \frac{3+\mu}{1-\mu}\rho^{-1})\cos\theta , \quad N_3 = \left(\rho^3 - \frac{3+\mu}{1-\mu}\rho^{-1}\right)\sin\theta , \tag{4.87}$$

$$\left.\begin{aligned} N_{i+1} &= f_{k1}(\rho)\cos k\theta \\ N_{i+2} &= f_{k1}(\rho)\sin k\theta \end{aligned}\right\} \quad f_{k1}(\rho) = \frac{3+\mu}{k(1-\mu)}\rho^k + \frac{1}{\rho^{k-2}} - \frac{k-1}{k}\rho^{-k} , \quad k = 2,3,\cdots, \tag{4.88}$$

$$\left.\begin{aligned} N_{i+1} &= f_{k2}(\rho)\cos k\theta \\ N_{i+2} &= f_{k2}(\rho)\sin k\theta \end{aligned}\right\} \quad f_{k2}(\rho) = \rho^{k+2} - \frac{k+1}{k}\rho^k - \frac{3+\mu}{k(1-\mu)}\rho^{-k} , \quad k = 2,3,\cdots . \tag{4.89}$$

Finding of the particular solution $\breve{w}$ is also elementary and includes expansion of the prescribed load $\overline{q}$ and/or the non-homogeneous boundary conditions at $r=b$ into a trigonometric series of sin $k\theta$ and cos $k\theta$. For the free boundary hole considered above with a uniform load $\overline{q}$, the particular solution $\breve{w}$ is

$$\breve{w} = \frac{\overline{q}b^4}{64D}\left(\rho^4 + 2\frac{3+\mu}{1+\mu}\rho^2 - 8\rho^2\ln\rho\right). \tag{4.90}$$

4.9 Extension to thin plates on elastic foundation

4.9.1 Basic equations

In the case of a plate resting on an elastic foundation, the left-hand side of eqn (4.17) and the boundary equation (4.16) must be augmented by the terms Kw and $-\alpha G_p w$, respectively:

$$D\nabla^4 w + Kw = \overline{q} , \qquad (\text{in } \Omega), \tag{4.91}$$

$$M_n = M_{ij}n_i n_j - \alpha G_p w = \overline{M}_n , \qquad (\text{on } \Gamma_M), \tag{4.92}$$

where $\alpha = 0$ for a Winkler-type foundation, $\alpha = 1$ for a Pasternak-type foundation, and the reaction operator

$$K = \begin{cases} k_w & \text{for Winkler stype foundation,} \\ (k_P - G_p\nabla^2) & \text{for Pasternak type foundation,} \end{cases} \tag{4.93}$$

with k_w being the coefficient of a Winkler-type foundation, k_P and G_P being the coefficient and shear modulus of a Pasternak-type foundation. The main difference between these two foundations is whether the effect of shear interactions is included.

4.9.2 T-complete functions and particular solutions

To obtain the T-complete functions for eqn (4.91), consider the following equation

$$D\nabla^4 f + Kf = D(\nabla^2 + C_1)(\nabla^2 - C_2) f = 0, \tag{4.94}$$

where

$$C_1 = C_2 = i\sqrt{k_w / D}, \tag{4.95}$$

for a Winkler-type foundation, and

$$C_1 = -\frac{G_P}{2D} - \sqrt{\left(\frac{G_P}{2D}\right)^2 - \frac{k_P}{D}}, \quad C_2 = \frac{G_P}{2D} - \sqrt{\left(\frac{G_P}{2D}\right)^2 - \frac{k_P}{D}}, \tag{4.96}$$

for a Pasternak-type foundation, and $i = \sqrt{-1}$.

To find the solution of eqn (4.94), we set

$$(\nabla^2 - C_2) f = A. \tag{4.97}$$

It follows from eqn (4.94) that

$$(\nabla^2 + C_1) A = 0. \tag{4.98}$$

Equation (4.98) is a Bessel equation and the T-complete functions can be generated in the following sequence:

$$A_{2m} = J_m(r\sqrt{C_1})\sin m\theta, \quad A_{2m+1} = J_m(r\sqrt{C_1})\cos m\theta, \qquad m = 0,1,2,\cdots, \tag{4.99}$$

in which $J_m(\,)$ is the Bessel function of the first kind with order *m*:

$$J_m(r) = \sum_{k=0}^{\infty} \frac{(-1)^k}{k!\Gamma(m+k+1)}\left(\frac{r}{2}\right)^{m+2k}, \tag{4.100}$$

with

$$\Gamma(x) = \int_0^{\infty} e^{-s} s^{x-1} ds. \tag{4.101}$$

In the same manner, let

$$(\nabla^2 + C_1) f = B \,. \tag{4.102}$$

Then we have

$$(\nabla^2 - C_2) B = 0 \,. \tag{4.103}$$

This is a modified Bessel equation and its T-complete solutions can be generated from the following sequence:

$$B_{2m} = I_m(r\sqrt{C_2})\sin m\theta, \quad B_{2m+1} = I_m(r\sqrt{C_2})\cos m\theta \,, \quad (m = 0,1,2,\cdots), \tag{4.104}$$

where $I_m(\,)$ is the modified Bessel function of the first kind with order m:

$$I_m(r) = \sum_{k=0}^{\infty} \frac{1}{k!\Gamma(m+k+1)} \left(\frac{r}{2}\right)^{m+2k} \,. \tag{4.105}$$

Subtracting eqn (4.97) from eqn (4.102) and using eqns (4.99) and (4.104) yields the T-complete solution for eqn (4.94):

$$f(r,\theta) = a_0 f_0(r) + \sum_{m=1}^{\infty} [a_m f_m(r)\cos m\theta + b_m f_m(r)\sin m\theta] \,, \tag{4.106}$$

where $f_m(r) = I_m(r\sqrt{C_2}) - J_m(r\sqrt{C_2})$, and the associated internal function N_j can be taken as

$$N_1 = f_0(r), \; N_{2m} = f_m(r)\cos m\theta, \; N_{2m+1} = f_m(r)\sin m\theta \,, \quad (m = 1,2,\cdots). \tag{4.107}$$

In this case the particular solution $\breve{w}$ is given by

$$\breve{w} = \int_{\Omega} \bar{q} w^*(r_{PQ}) d\Omega \,, \tag{4.108}$$

where

$$w^*(r_{PQ}) = \frac{1}{C_1 + C_2} \left[\frac{K_0(r_{PQ}\sqrt{C_2})}{2\pi D} - \frac{Y_0(r_{PQ}\sqrt{C_1})}{4D} \right], \tag{4.109}$$

with $K_0(\,)$ being the modified Bessel function of the second kind with zero order and $Y_0(\,)$ being the Bessel function of the second kind with zero order.

4.9.3 Variational formulation

The variational functional used for deriving HT FE formulation of thin plates on an elastic foundation has the same form as that of eqn (4.46), i.e.,

$$\Pi_m = \sum_e \{\Pi_e - \int_{\Gamma_{e2}} (\overline{M}_n - M_n) w_{,n} ds + \int_{\Gamma_{e4}} (\overline{R} - R) w ds + \int_{\Gamma_{e5}} (M_n \tilde{w}_{,n} - R\tilde{w}) ds\}, \tag{4.110}$$

except that the complementary energy density U in eqn (4.48) is replaced by U^*:

$$U^* = \frac{1}{2D(1-\mu^2)}[(M_{11} + M_{22})^2 + 2(1+\mu)(M_{12}^2 - M_{11}M_{22})] + V^*, \tag{4.111}$$

where

$$V^* = \begin{cases} \dfrac{k_w w^2}{2} & \text{for a Winkler type foundation,} \\ \dfrac{1}{2}(k_P w^2 + G_P w_{,i} w_{,i}) & \text{for a Pasternak type foundation.} \end{cases} \tag{4.112}$$

Using the Gauss divergence theorem and the properties of the internal trial function, eqn (4.110) can be simplified to:

$$\Pi_{me} = \frac{1}{2}\int_{\Omega_e} \overline{q} w d\Omega + \int_{\Gamma_{e1}} M_n \overline{w}_{,n} ds - \int_{\Gamma_{e3}} R\overline{w} ds + \int_{\Gamma_{e2}} (M_n - \overline{M}_n) w_{,n} ds - \int_{\Gamma_{e4}} (R - \overline{R}) w ds + \frac{1}{2}\int_{\Gamma_e} (Rw - M_n w_{,n}) ds - \int_{\Gamma_{e5}} (R\tilde{w} - M_n \tilde{w}_{,n}) ds, \tag{4.113}$$

which is exactly the same as eqn (4.53). Hence, the problem can be treated in the same manner as for thin plate bending without foundation.

4.10 Two alternative plate bending *p*-elements

In the previous sections of this chapter, we discussed thin plate bending T-elements with three DOF (one deflection and two rotation components) at corner nodes and an optional number of hierarchical side mode DOF associated with mid-side nodes. Other types of thin plate bending T-elements, such as the element with only one DOF at corner nodes, are possible. In this section we describe two alternative plate bending *p*-elements with 1 and 6 DOF respectively at corner nodes, which were presented by Jirousek *et al.* [11] in 1997. It should be mentioned that these two alternative element models differ from the previous ones only by the frame definitions. Therefore we present here only the definitions of frame functions $\tilde{w}$ and $\tilde{w}_{,n}$ for simplicity.

4.10.1 Element with one DOF at corner nodes

A particular element side A-C-B (Fig. 1.3) is considered and appropriate definitions of the sub-vectors $\mathbf{d}_A, \mathbf{d}_B, \mathbf{d}_C$ of the vector $\mathbf{d}$ and of the functions $\tilde{w}$ and $\tilde{w}_{,n}$ are given. In the case of one DOF at corners, the sub-vectors $\mathbf{d}_A, \mathbf{d}_B, \mathbf{d}_C$ are defined by

$$\mathbf{d}_A = w_A, \quad \mathbf{d}_B = w_B \quad \text{and} \quad \mathbf{d}_C = \{\Delta w_{,nC1}, \Delta w_{C1}, \Delta w_{,nC2}, \cdots\}^T, \qquad (4.114)$$

where the parameters $\Delta w_{,nC1}, \Delta w_{C1}, \Delta w_{,nC2}, \cdots$, etc., associated for convenience with the mid-side node *C*, correspond to hierarchical side-modes. Hence the frame functions $\tilde{w}$ and $\tilde{w}_{,n}$ along the side A-C-B can be written as

$$\begin{aligned} \tilde{w} &= \tilde{N}_1 w_A + \tilde{N}_2 w_B + \tilde{N}_3 \Delta w_{C1} + \tilde{N}_5 \Delta w_{C2} + \cdots \\ &= \tilde{N}_1 w_A + \tilde{N}_2 w_B + \sum_{k=1,2,\cdots} \tilde{N}_{2k+1} \Delta w_{Ck}, \end{aligned} \qquad (4.115)$$

$$\tilde{w}_{,n} = \tilde{N}_4 \Delta w_{,nC1} + \tilde{N}_6 \Delta w_{,nC2} + \cdots = \sum_{k=1,2,\cdots} \tilde{N}_{2k+2} \Delta w_{,nCk}, \qquad (4.116)$$

where $\tilde{N}_1$ and $\tilde{N}_2$ are defined in eqn (2.27), and

$$\tilde{N}_{2k+1} = \xi^{k-1}(1-\xi^2), \quad \tilde{N}_{2k+2} = \xi^{k-1}, \qquad (k=1,2,\ldots). \qquad (4.117)$$

4.10.3 Element with six DOF at corner nodes

For this type of element, the sub-vectors of nodal parameter have the following definition:

$$\mathbf{d}_A = \left\{ w_A \quad w_{xA} \quad w_{yA} \quad w_{xxA} \quad w_{xyA} \quad w_{yyA} \right\}^T, \qquad (4.118)$$

$$\mathbf{d}_B = \left\{ w_B \quad w_{xB} \quad w_{yB} \quad w_{xxB} \quad w_{xyB} \quad w_{yyB} \right\}^T, \qquad (4.119)$$

and $\mathbf{d}_C$ is defined in eqn (4.114). In this case, the frame functions $\tilde{w}$ and $\tilde{w}_{,n}$ along the side A-C-B have the following definitions:

$$\begin{aligned} \tilde{w} = {} & \tilde{N}_1 w_A + \tilde{N}_2 w_{\xi A} + \tilde{N}_3 w_{\xi\xi A} + \tilde{N}_4 w_B \\ & + \tilde{N}_5 w_{\xi B} + \tilde{N}_6 w_{\xi\xi B} + \sum_{k=1,2,\cdots} \tilde{N}_{2k+9} \Delta w_{Ck}, \end{aligned} \qquad (4.120)$$

$$\tilde{w}_{,n} = \tilde{N}_7 w_{,nA} + \tilde{N}_8 w_{,n\xi B} + \tilde{N}_9 w_{,nB} + \tilde{N}_{10} \Delta w_{,n\xi B} + \sum_{k=1,2,\cdots} \tilde{N}_{2k+10} \Delta w_{,nCk}, \qquad (4.121)$$

where the subscript ξ represents the differentiation of the corresponding function with respect to the non-dimensional coordinate 'ξ', varying from –1 to +1 between *A* and *B*, and functions $\tilde{N}_i$ are defined as [11]

$$\tilde{N}_1 = \frac{1}{16}(-3\xi^5 + 10\xi^3 - 15\xi + 8),$$

$$\tilde{N}_2 = \frac{1}{16}(-3\xi^5 + \xi^4 - 10\xi^3 - 6\xi^2 - 7\xi + 5),$$

$$\tilde{N}_3 = \frac{1}{16}(-\xi^5 + \xi^4 + 2\xi^3 - 2\xi^2 - \xi + 1),$$

$$\tilde{N}_4 = \frac{1}{16}(3\xi^5 - 10\xi^3 + 15\xi + 8),$$

$$\tilde{N}_5 = \frac{1}{16}(-3\xi^5 - \xi^4 + 10\xi^3 + 6\xi^2 - 7\xi - 5),$$

$$\tilde{N}_6 = \frac{1}{16}(\xi^5 + \xi^4 - 2\xi^3 - 2\xi^2 + \xi + 1),$$

$$\tilde{N}_7 = \frac{1}{4}(\xi^3 - 3\xi + 2), \qquad \tilde{N}_8 = \frac{1}{4}(\xi^3 - \xi^2 - \xi + 1),$$

$$\tilde{N}_9 = \frac{1}{4}(-\xi^3 + 3\xi + 2), \qquad \tilde{N}_{10} = \frac{1}{4}(\xi^3 + \xi^2 - \xi - 1),$$

$$\tilde{N}_{2k+9} = \xi^{k-1}(1-\xi^2)^3, \qquad \tilde{N}_{2k+10} = \xi^{k-1}(1-\xi^2)^2. \tag{4.122}$$

The 'local' parameters $w_{\xi A}, w_{\xi B}$ and $w_{,nA}\ w_{,nB}$ in eqns (4.120) and (4.121) may be expressed as follows in terms of the global parameters w_{xA}, w_{xB}, w_{yA} and w_{yB}:

$$w_{\xi A} = -\frac{l_{AB}}{2}(w_{xA}n_y - w_{yA}n_x), \qquad w_{\xi B} = -\frac{l_{AB}}{2}(w_{xB}n_y - w_{yB}n_x), \tag{4.123}$$

and

$$w_{,nA} = w_{xA}n_x + w_{yA}n_y, \quad w_{,nB} = w_{xB}n_x + w_{yB}n_y. \tag{4.124}$$

Moreover, for the higher order 'local' parameters, $w_{\xi\xi A}, w_{\xi\xi B}$ and $w_{,n\xi A}\ w_{,n\xi B}$ apply the following relations:

$$w_{\xi\xi A} = \frac{l_{AB}^2}{4}(w_{xxA}n_y^2 - w_{xyA}n_x n_y + w_{yyA}n_x^2), \tag{4.125a}$$

$$w_{\xi\xi B} = \frac{l_{AB}^2}{4}(w_{xxB}n_y^2 - w_{xyB}n_x n_y + w_{yyB}n_x^2)\,, \tag{4.125b}$$

and

$$w_{,n\xi A} = -\frac{l_{AB}}{2}[w_{xxA}n_x n_y - (n_x^2 - n_y^2)w_{xyA} - n_x n_y w_{yyA}], \tag{4.126a}$$

$$w_{,n\xi B} = -\frac{l_{AB}}{2}[w_{xxB}n_x n_y - (n_x^2 - n_y^2)w_{xyB} - n_x n_y w_{yyB}]\,. \tag{4.126b}$$

4.10.4 Implementation

As was noted previously, it is important to choose the proper number of m in the internal field (4.18). The rank condition (2.51) in this case reads

$$m \geq k - 3\,. \tag{4.127}$$

Though the use of the minimal m=k–3 does not always guarantee a stiffness matrix with the full rank of (k–3), full rank may always be achieved by suitably augmenting m. Table 4.1 shows the minimum number m for a quadrilateral element with one or six DOF at the corner nodes and an optional number M of side mode DOF [11].

For a quadrilateral element with n=1 or 6 DOF at corner nodes and M=1,3,5,… etc. hierarchical DOF at mid-side nodes, the element will present a $k \times k$ stiffness matrix in which k is equal to

$$k = 4(n + M)\,. \tag{4.128}$$

The standard eigenvalues tests [11] have shown that while the quadrilateral element with one DOF at the element corners the minimum of homogeneous solutions N_i in eqn (4.18), namely

$$m = k - 3\,, \qquad (\text{if } n\text{=}1), \tag{4.129}$$

warrants a stiffness matrix with full rank, in the case of 6 DOF at the element corners two additional homogeneous solutions are necessary

$$m = k - 1\,, \qquad (\text{if } n\text{=}6), \tag{4.130}$$

to ensure the stiffness matrix **k** with full rank. Indeed, with m=k–3, the element stiffness matrix may present a spurious zero energy mode.

In order to ensure that the orientation of the non-dimensional coordinate ξ will be the same for the inter-element portion of the boundary between two elements, the simplest method consists of choosing the nodes A ($\xi_A = -1$) and B ($\xi_B = +1$) (Fig. 1.3) so that the corresponding global numbers N_{oA} and N_{oB} of these nodes in the FE mesh fulfill the condition

$$N_{oA} < N_{oB}\,. \tag{4.131}$$

Furthermore, it is of interest to observe that the side-mode hierarchical DOF in $\mathbf{d}_C$ (eqn (4.114)) are arranged so that the polynomial degree of the frame is alternatively increased for the normal slope $\tilde{w}_{,n}$ and the deflection $\tilde{w}$. In order to keep the polynomial degree of $\tilde{w}_{,n}$ one degree lower than that ($\tilde{p}$) of the deflection $\tilde{w}$, we begin by improving $\tilde{w}_{,n}$ (M=1) and then upgrading M by steps of two.

Table 4.1. Numbers m, M, p and $\tilde{p}$ for two families of a quadrilateral element with one or six DOF at the corner nodes and an optional number M of side-mode DOF. $\tilde{p}$ and p: polynomial degree of frame function $\tilde{w}$ and polynomial degree of internal field w in eqn (4.18).

Quantity	N	k number of element's DOF								
		16	24	28	32	36	40	44	48	52
m	1	13	21	-	29	-	37	-	45	-
	6	-	-	27	-	35	-	43	-	51
M	1	3	5	-	7	-	9	-	11	-
	6	-	-	1	-	3	-	5	-	7
p	1	5	7	-	9	-	11	-	13	-
	6	-	-	8	-	10	-	12	-	14
$\tilde{p}$	1	2	3	-	4	-	5	-	6	-
	6	-	-	5	-	6	-	7	-	8

4.11 Numerical examples and assessment

In this section various results of numerical studies are presented and, whenever available, compared with results of other methods extracted from the literature. Most of the numerical studies presented refer to the conventionally used square plate test. Unless stated otherwise, information about the mesh density concerns a symmetric quadrant of the plate. Furthermore, a Poisson ratio of μ=0.3 has been used in most of the examples.

4.11.1 Simply supported square plate

The first example is a simply supported square plate with span to thickness ratio L/t=1000. The plate is subjected to a uniform load q. Numerical results for central deflections and central moments for different mesh densities are displayed in Table 4.2. It can be observed that the present 12 DOF quadrilateral element yields more accurate results here than the well known 12 DOF discrete-Kirchhoff thin plate element [2].

The second example is again a simply supported square plate, but is subjected

Table 4.2. Deflections and moments at the centre of the simply supported square plate.

Mesh	$10^2 Dw_c : qL^4$			$10M_{11c} : qL^2$		
	DKQ	Q4BL	Present	DKQ	Q4BL	Present
1×1	0.37847	-	0.38958	0.6031	-	0.47282
2×2	0.40456	0.40355	0.40567	0.5010	0.47125	0.47842
4×4	0.40600	0.40584	0.40630	0.4839	0.47732	0.47874
8×8	0.40619	0.40616	0.40626	0.4801	0.47850	0.47886
16×16	0.40622	0.40622	0.40624	0.4792	0.47877	0.47886
Exact		0.406235			0.47886	

Note: DKQ, Batoz and Tahar [2]; Q4BL, Zienkiewicz *et al*. [22].

Table 4.3. Centrally loaded simply supported square plate. Central load taken as nodal load (*n*=DOF at corners, k=Number of lines and columns of element stiffness matrix).

Quantity		$\frac{10Dw_{centre}}{PL^2}$			$\frac{R_{corner}}{P}$		
n		1	3	6	1	3	6
k	16	0.128353	0.111309	-	0.040028	0.122717	-
	24	0.120348	0.115109	-	0.071255	0.105090	-
	28	-	-	0.115688	-	-	0.119944
	32	0.117948	0.115747	-	0.076547	0.104234	-
	36	-	-	0.115893	-	-	0.119656
	40	0.117042	0.115898	-	0.082357	0.103679	-
	44	-	-	0.115974	-	-	0.119826
	48	0.116648	0.115969	-	0.087149	0.103932	-
	52	-	-	0.116003	-	-	0.119782
Exact		0.116008			0.121905		

to a concentrated load *P* at the centre of the plate. The example was taken from [11]. The purpose of this example is to show the performance of *p*-elements described in the previous section. In the analysis, a 2×2 HT p-element mesh is used to model the whole plate. The concentrated load *P* was considered either as a nodal load (Table 4.3 and 4.4) or assumed uniformly distributed over a small circular area with radius $b=L/1000$ (Table 4.5 and 4.6) and accounted for by the discontinuous particular solution (eqns (4.44) and (4.45)). The comparison of results clearly shows the superiority of the latter approach over the former one. It

is also found from Table 4.4 that the results obtained by the element models with 3 or 6 DOF at corner nodes are more accurate than those from the one with one DOF at corners in this example. However, Table 4.6 shows that the element models with 1 and 6 DOF at corners can provide better results than those from the one with 3 DOF at corners when the expressions (4.44) and (4.45) are used to calculate the particular solution $\breve{w}$.

Table 4.4. Percentage errors in HT p-elements displayed in Table 4.3.

Quantity		Δw_{centre} %			R_{corner} %		
n		1	3	6	1	3	6
	16	10.64	–4.05	-	–67.16	0.67	-
	24	3.74	–0.78	-	–41.55	–37.21	-
	28	-	-	–0.28	-	-	–1.61
k	32	1.67	–0.23	-	–37.21	–14.42	-
	36	-	-	–0.10	-	-	–1.85
	40	0.98	–0.10	-	–32.44	–14.95	-
	44	-	-	–0.03	-	-	–1.71
	48	0.55	–0.03	-	–28.51	–14.74	-
	52	-	-	0.00	-	-	–1.74

Table 4.5. Centrally loaded simply supported square plate. Central load assumed uniformly distributed over a circular area with radius $b=L/1000$ (*n*=DOF at corners, k=Number of lines and columns of element stiffness matrix).

Quantity		$\frac{10Dw_{centre}}{PL^2}$			$\frac{R_{corner}}{P}$		
n		1	3	6	1	3	6
	16	0.116544	0.111704	-	0.113772	0.114929	-
	24	0.116278	0.115013	-	0.122840	0.129124	-
	28	-	-	0.115594	-	-	0.120907
k	32	0.116133	0.115635	-	0.119159	0.126481	-
	36	-	-	0.115813	-	-	0.121054
	40	0.116053	0.115829	-	0.120250	0.124126	-
	44	-	-	0.115902	-	-	0.121546
	48	0.116032	0.115911	-	0.121488	0.122715	-
	52	-	-	0.115946	-	-	0.121688
Exact		0.116008			0.121905		

Table 4.6. Percentage errors in HT *p*-elements displayed in Table 4.5.

Quantity		Δw_{centre} %			R_{corner} %		
n		1	3	6	1	3	6
	16	0.46	–3.71	-	–6.67	18.89	-
	24	0.23	–0.86	-	0.77	5.92	-
	28	-	-	–0.36	-	-	–0.82
k	32	0.11	–0.32	-	–2.25	3.75	-
	36	-	-	–0.17	-	-	–0.70
	40	0.04	–0.15	-	–1.36	1.82	-
	44	-	-	–0.09	-	-	–0.29
	48	0.02	–0.08	-	–0.34	0.66	-
	52	-	-	–0.05	-	-	–0.18

4.11. 2 Plates on an elastic foundation

To demonstrate the application of T-elements to the problem of thin plates on an elastic foundation, two simple examples are considered here. One is a square plate on a Winkler-type foundation, and the other is again a square plate but on a Pasternak-type foundation.

(a) *A square plate on a Winkler medium* (Fig. 4.7)

A square plate with two adjacent edges fixed and the remaining edges simply supported on a Winkler-type foundation is subjected to a uniform load *q*. The initial data are as follows:

$$L = 100\,\text{cm},\ k_w = 5\,kg/\text{cm}^3,\ t = 1\,\text{cm},\quad \mu = 0.3,\quad E = 2\times10^6\ \text{kg/cm}^2\,.$$

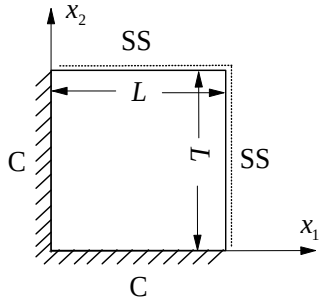

Fig. 4.7: Square plate with two adjacent edges clamped (C) and the others simply supported (SS) on a Winkler medium.

The plate is analyzed with several finite element meshes ($N\times N$, N=2,4,6). Elements of both the present HT FE model and the conventional displacement model (C-DM) [22] are tested. The results for the normal bending moments on one of the two clamped boundaries, say the boundary x_2=0, M_n ($M_n=\beta qa^2$) are displayed in Table 4.7. It can be seen that the difference between the two FE models diminishes with refinement of the element meshes. For a small value of N, however, the HT FE formulation seems to be more accurate than the conventional approach.

Table 4.7. Bending moment coefficients β for a square plate on a Winkler-medium on the line x_2=0.

Method	mesh	$x_1 = 0.2L$	$0.4L$	$0.6L$	0.8L
HT FE	2×2	–0.01058	–0.1862	–0.2030	–0.01438
	4×4	–0.01113	–0.1914	–0.2085	–0.01489
	6×6	–0.01169	–0.1975	–0.2113	–0.01510
C-DM	2×2	–0.01012	–0.1799	–0.1988	–0.01375
	4×4	–0.01102	–0.1901	–0.2069	–0.01463
	6×6	–0.01165	–0.1973	–0.2110	–0.01507
Exact [21]		–0.01193	–0.1986	–0.2122	–0.01510

(b) *A square plate on a two-parameter foundation*

The example produces the results appearing in [19] of a simply supported square plate on a two-parameter foundation with side length L and modulus of elastic foundation K_P ($=k_PL^4/D$)=200. The plate is subjected to a uniform load q.

Table 4.8. Central deflections and moments for a square plate on a Pasternak-type foundation with $K_P = 200,\ t/L = 0.005$ and $\mu = 0.25$.

Method	mesh	$10^2 Dw_c : qL^4$		$10^2 M_{11c} : qL^2$	
		g_P =5	g_P =20	g_P =5	g_P =20
HT FE	2×2	0.2133	0.1472	2.3132	1.5105
	4×4	0.2212	0.1533	2.3965	1.5887
	6×6	0.2259	0.1562	2.4101	1.6089
C-DE	2×2	0.2079	0.1421	2.2813	1.4739
	4×4	0.2198	0.1519	2.3603	1.5696
	6×6	0.2256	0.1561	2.4093	1.6080
BEM[a]		0.2250	0.1560	2.4066	1.6064
Exact [20]		0.2264	0.1568	2.4179	1.6129

[a]The results are obtained by the boundary element method with 32 elements [20].

Owing to the symmetry of the problem only one quadrant of the plate is modelled by meshes ($N\times N$, N=2,4,6) and analyzed by both HT FE and C-DE codes. The results for central deflections w_c and central bending moments M_{11c} are shown in Table 4.8 for different values of $g_P(=G_P L^2/D)$, and comparison is made with the results obtained by the boundary element method [20].

It can be seen from Tables 4.7 and 4.8 that the HT FE results for plates on elastic foundation are in good agreement with other solutions. As expected for the above two examples, it is found from the numerical results that the deflections and moments converge gradually to the analytical results along with refinement of the element meshes.

4.11.3 Sensitivity to mesh distortion

The numerical study on the sensitivity to mesh distortion is performed for thin plate with distorted 4×4 and 8×8 meshes as shown in Fig. 4.8. It should be mentioned that the mesh density is indicated here for the whole plate rather than a symmetric quadrant as used in Section 4.10.1.

As a measure of sensitivity to mesh distortion, we consider the percentage error ε% defined as

$$\varepsilon\% = 100\times\frac{r_U - r_D}{r_U}, \tag{4.132}$$

where r_U and r_D stand for the uniform and the distorted mesh results respectively. The percentage errors displayed in Table 4.9 for deflection and moments at the centre of the plate show that the results are not overly sensitive to mesh distortion. This feature, typical for all T-elements, is attributable to the fact that the internal Trefftz field w, defined in a local Cattesian coordinate system, does not depend on mesh distortion.

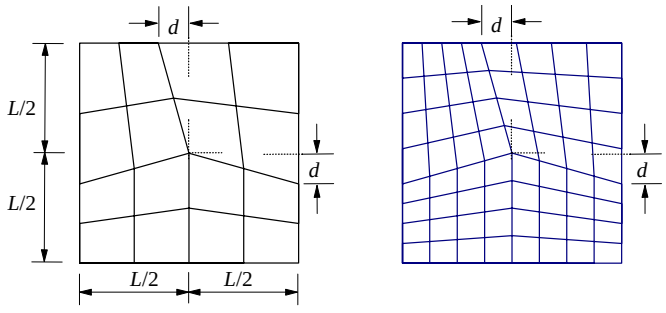

Fig. 4.8: Distorted 4×4 and 8×8 meshes of T-elements.

Table 4.9. Percentage error ε% due to distortion of 4×4 and 8×8 meshes for a uniformly loaded simply supported square plate.

Mesh		4×4	8×8	
L/t	Quantity	*L/d*=8	*L/d*=8	*L/d*=4
	w_c	–0.442	–0.092	–0.205
100	M_{11c}	–1.143	–0.387	–1.037
	M_{22c}	–1.231	–0.399	–0.934
	w_c	–0.445	–0.091	–0.203
1000	M_{11c}	–1.139	–0.387	–1.036
	M_{22c}	–1.232	–0.395	–0.934

4.11.4 Optimal number of trial functions

It is important to study in more detail the problem of choosing the proper number *m* of trial functions **N** and *M* of DOF associated with mid-side nodes for a *p*-method element in order to obtain the maximum efficiency from the *p*-version of T-element model. The numerical assessment of this problem has been reported by Jirousek [6] and we follow most of his results in this subsection.

It should be mentioned that the basic rule (4.32) indicates only the minimal number of trial functions to prevent spurious energy modes. Moreover, it is also desirable that geometrical isotropy (independence from the rotation of the coordinate axis) be preserved when the series is truncated. When the standard polynomial functions (4.30) are used, then as pointed out in [8], the latter condition is fulfilled if the series is truncated after either the two biharmonic terms ($r^2 \operatorname{Re} z^k, r^2 \operatorname{Im} z^k$) or the two harmonic terms ($\operatorname{Re} z^k, \operatorname{Im} z^k$), a condition which results in using uneven values for *m* (since *k*=0 the sequence (4.30) yields only three independent functions). The optimal value of *m* for a given degree of *p*-refinement should, however, be found by numerical experimentation.

The effect of *M* on computational accuracy is shown in Fig. 4.9. It shows the decrease in percentage error when *M* is varied from 1 to 7 (at the same time, the number *m* of **N**'s is suitably augmented following the rule given in Table 4.10). Note that the DOF associated with the mid-side nodes are ranged in the following order: $b_{C1}, a_{C1}, b_{C2,} a_{C2}, b_{C3}, \cdots$. This indicates that the terms b_{Ci} are considered prior to the terms a_{Ci}. The purpose of this arrangement is to improve the accuracy of the normal slope $\tilde{w}_{,n}$.

It is found from Fig. 4.9 that the solution error decreases quickly along with the increase of *M*. It should also be mentioned that a considerable improvement in accuracy, as compared with the 12 DOF hybrid-Trefftz quadrilateral element in [8] is achieved already by introducing a single DOF (*M*=1) at the element mid-side nodes. This leads to improving the linear distribution of the normal slope $\tilde{w}_{,n}$ by a quadratic term and results in an equal order of polynomial approximation for $\tilde{w}_{,s}$ and $\tilde{w}_{,n}$.

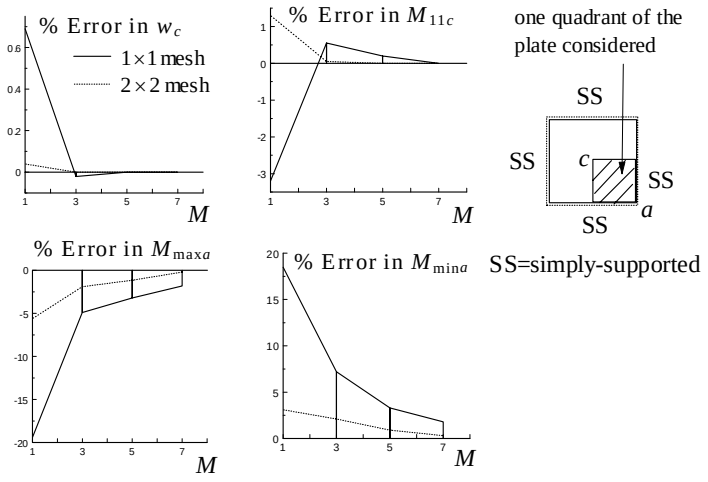

Fig. 4.9: Convergence study of uniformly loaded SS plate.

It is worth noting that in the above numerical test of the uniformly refined quadrilateral *p*-elements (the number *M* was uniformly increased at all mid-side nodes) each *M* was combined with the minimal number of trial functions **N** (*m*=13,21,29 and 37 for *M*=1,3,5,7) which, incidentally, also satisfied the condition of general isotropy.

Some additional results which show the effect of *m* and *M* on the solution accuracy are presented in Tables 4.10 and 4.11 for a uniformly loaded clamped square plate. From these numerical studies the following conclusions may be made:

(a) for the lowest order of refinement *M*=1, 15 trial functions frequently yield slightly better results than the minimal number of 13 functions;

(b) for *M*=3, the minimal number of 21 trial functions is the best;

(c) the minimum number of trial functions (29 for *M*=5) also yields very satisfactory results for higher order elements. Yet with 2 or 4 additional trial functions, still better results are usually obtained at sampling points situated at element centre nodes and at mid-side nodes, while at element corners the errors increase.

4.11.5 Morley's skew plate problem (Fig. 4.10)

The performance of a special purpose corner element in singularity calculations is exemplified by the analysis of the well-known Morley's skew plate problem (Fig. 4.10). For the skew plate angle of 30°, the plate exhibits a very strong singularity

at the obtuse corners (the exponent of the leading singularity term Cr^{λ} of the deflection expansion is equal to 1.2). Such a problem is considered difficult and has attracted the attention of research workers [1,6,19]. The difficulty is mainly due to the strong singularity at the obtuse corner which causes most FE models either to converge very slowly to the true solution, or not to converge at all. The analytical solution of the problem based on the series expansion with coefficients determined by the least square method was presented by Morley [12], whose results are generally used as reference.

Table 4.10. Effect of the order in which the terms of the approximating sequence of trial function **N** are truncated. Uniformly loaded clamped square plate, single element over a quadrant.

M=		1	3	5	7
m=		13	21	29	37
%	$w_{\max}$	5.43	–0.72	0.07	0.0
error	$M_{\max}$	36.82	–3.26	–1.02	–0.34
in	$M_{\min}$	–4.57	0.87	0.31	0.26

Note: The last two terms of **N** are chosen to be biharmonic.

Table 4.11. Variation of percentage error in terms of number of trial functions **N** used for various degrees of uniform *p*-refinement. Uniformly loaded clamped square plate.

Mesh Quantity for whole plate		M=	1			3			5	
		m=13*	15	17	m=21*	23	25	m=29*	39	41
2×2	w_A	5.435	5.435	5.123	–0.721	–0.703	–0.713	0.072	0.056	0.054
	$M_{11\,A}$	36.820	35.543	40.106	–3.262	–5.548	–5.932	–1.023	2.344	3.365
	M_{nB}	–4.573	–4.570	–4.623	0.872	1.975	–2.132	0.314	–1.756	–1.744
3×3	w_A	0.237	0.240	–0.251	0.012	–0.035	–0.28	0.002	0.000	0.000
	$M_{11\,A}$	1.324	0.976	2.135	–0.011	–0.108	–0.124	0.004	0.001	0.002
	M_{nB}	–9.84	–7.63	–7.62	0.063	0.059	0.030	0.058	0.049	0.036

Note: sampling point A, plate centre; B, plate mid-edge; * stands for minimum number of trial functions for a given degree of element refinement.

The numerical results for different meshes (2×2, 3×3, 4×4 shown in Fig. 4.11) are obtained at the plate centre and displayed in Tables 4.12 and 4.13, which are compared with Morley's results (w_c= 0.000408qL^4/D, M_{11c}=0.0108qL^2 and M_{22c}=0.0191qL^2).

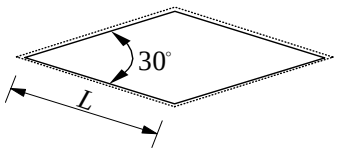

Fig. 4.10: Uniformly loaded simply supported 30° skew plate (L/t=100).

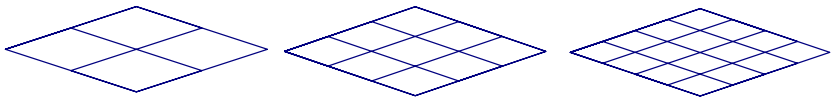

Fig. 4.11: Configuration of meshes used in finite element analysis.

Table 4.12. Solution with special purpose corner functions applied to all corner elements for Morley's simply supported uniformly loaded skew 30° plate.

Mesh	Quantity	Percentage error			
		M=1	3	5	7
2×2	w_c	–6.08	0.55	0.0	0.0
	M_{11c}	–5.03	3.32	1.08	0.01
	M_{22c}	–27.86	5.44	0.97	0.03
3×3	w_c	–1.98	0.31	0.0	0.0
	M_{11c}	0.92	0.27	0.0	0.0
	M_{22c}	3.25	1.02	0.03	0.0
4×4	w_c	–1.58	0.01	0.0	0.0
	M_{11c}	0.39	0.11	0.0	0.0
	M_{22c}	2.25	0.98	0.01	0.0

The high efficiency of special purpose corner functions for the solution of singularity problems can be seen from the Tables 4.12 and 4.13. Such functions play an even more important role within the T-element model where, by definition, the expansion basis of each element is optional. This enables involved singularity or stress concentration problems to be efficiently solved without troublesome mesh refinement. It is also evident from the two tables above that the T-element model performs well with regard to *p*-convergence; i.e. the numerical results converge quickly to the analytical results along with increase of *M*.

Table 4.13. Solution without special purpose corner functions for Morley's simply supported uniformly loaded skew plate.

Mesh	Quantity	Percentage error			
		M=1	3	5	7
2×2	w_c	–29.45	–6.44	1.46	–1.22
	M_{11c}	–7.45	–7.33	–3.44	–1.55
	M_{22c}	–22.52	–9.89	5.78	3.67
3×3	w_c	–22.98	–4.88	–1.98	0.44
	M_{11c}	–9.55	–6.78	–1.59	–0.76
	M_{22c}	–23.45	–11.55	–2.66	1.65
4×4	w_c	–19.65	–3.98	–1.79	0.34
	M_{11c}	–8.22	–4.95	–1.22	–0.62
	M_{22c}	–19.55	–5.88	3.53	2.12

References

[1] Argyris, J.H. & Lochner, N. On the application of SHEBA shell element. *Comp. Meth. Appl. Mech. Eng.*, **1**, pp. 317-347, 1972.

[2] Batoz, J.L. & Tahar, M.B. Evaluation of a new quadrilateral thin plate bending element. *Int. J. Numer. Meth. Eng.*, **18**, pp. 1655-1677, 1982.

[3] Brebbia, C.A., Telles, J.C.F. & Wrobel, L.C. *Boundary element Techniques: Theory and applications in engineering*, Springer-Verlag: Berlin, 1984.

[4] Herrera, I. *Boundary Method: An algebraic theory*, Pitman: Boston, 1984.

[5] Jin, W.G., Cheung, Y.K. & Zienkiewicz, O.C. Trefftz method for Kirchhoff plate bending problems. *Int. J. Numer. Meth. Eng.*, **36**, pp. 765-781, 1993.

[6] Jirousek, J. Hybrid-Trefftz plate bending elements with *p*-method capabilities. *Int. J. Numer. Meth. Eng.*, **24**, pp. 1367-1393, 1987.

[7] Jirousek, J. Improvement of computational efficiency of the 9 DOF triangular hybrid-Trefftz plate bending element. *Int. J. Numer. Meth. Eng.*, **23**, pp. 2167-2168, 1986.

[8] Jirousek, J. & Guex, L. The hybrid-Trefftz finite element model and its application to plate bending. *Int. J. Numer. Meth. Eng.*, **23**, pp. 651-693, 1986.

[9] Jirousek, J. & Leon, N. A powerful finite element for plate bending. *Comp. Meth. Appl. Mech. Eng.*, **12**, pp. 77-96, 1977.

[10] Jirousek, J., Wroblewski, A. & Szybinski, B. A new 12 DOF quadrilateral element for analysis of thick and thin plates. *Int. J. Numer. Meth. Eng.*, **38**, pp. 2619-2638, 1995.

[11] Jirousek, J., Wroblewski, A. & Szybinski, B. Alternative displacement frame formulations in hybrid-Trefftz Kirchhoff plate *p*-elements. *Computer*

Assisted Mechanics and Engineering Sciences, **4**, pp. 417-451, 1997.
[12] Morley, L.S.D. *Skew Plates and Structures*, Pergamon Press: London, 1963.
[13] Qin, Q.H. Hybrid Trefftz finite element approach for plate bending on an elastic foundation. *Appl. Mathe. Modelling*, **18**, pp. 334-339, 1994.
[14] Qin, Q.H. Postbuckling analysis of thin plates by a hybrid Trefftz finite element method. *Comp. Meth. Appl. Mech. Eng*., **128**, pp. 123-136, 1995.
[15] Qin, Q.H. Transient plate bending analysis by hybrid-Trefftz element approach. *Communi. Numer. Meth. Eng*., **12**, pp. 609-616, 1996.
[16] Venkatesh, A. & Jirousek, J. An improved 9 DOF hybrid-trefftz triangular element for plate bending. *Engineering Comput*., **4**, pp. 207-222, 1987.
[17] Venkatesh, A. & Jirousek, J. Accurate representation of local effects due to concentrated and discontinuous loads in hybrid-Trefftz plate bending elements. *Compu. Struct*., **57**, pp. 863-870, 1995.
[18] Wah, T. Elastic quadrilateral plates. *Compu. Struct.*, **10**, pp. 457-466, 1979.
[19] Wang, D.W., Katz, I.N. & Szabo, B.A. *h*- and *p*-version finite element analysis of rhombic plate. *Int. J. Numer. Meth. Eng*., **20**, pp. 1399-1405, 1984.
[20] Wang, J., Wang, X.X. & Huang, M.K. Fundamental solutions and boundary integral equations for Reissner's plates on two-parameter foundations. *Int. J. Solids Struct*., **29**, pp. 1233-1239, 1992.
[21] Zhang, F.F. *The elastic thin plates*, Science Press of China: Beijing, pp. 98-102, 1984 (in Chinese).
[22] Zienkiewicz, O.C. & Taylor, R.L. *The finite element method*, 4th Edn, McGraw Hill: London, 1989.

Chapter 5

Thick Plates

5.1 Introduction

This chapter deals with the application of T-elements to thick plate problems. In contrast to Kirchhoff's thin plate theory, the transverse shear deformation effect of the plate is taken into account in thick plate theory, so that the governing equation is a sixth-order boundary value problem. As a consequence, three boundary conditions should be considered for each boundary. In contrast, Only two boundary conditions are considered in thin plate theory.

It is well-known that Kirchhoff's thin plate theory [25] demands both the deflection and normal rotations to be continuous between elements, i.e., C^1 continuous. This requirement makes it difficult to construct conforming elements. This difficulty can be bypassed using thick plate theory, usually Mindlin's theory [12] which is based on independent approximations for the deflections and rotations. Elements based on Mindlin's theory require only C^0 continuity, which is readily achieved. Moreover, the theory is applicable to both thick and thin plates [11]. Despite these advantages, there are a number of problems associated with thick plate elements. Specifically, the elements can lock as the plate thickness approaches zero, thereby giving incorrect results for thin plates. In addition, many elements have zero energy modes, which may cause spurious mechanisms to spread through the mesh. Many techniques, such as reduced integration, special shear interpolation and stabilization matrix, have been used to alleviate these problems. It has been shown that the use of hybrid-Trefftz thick plate elements can also eliminate these problems [10,11]. Based on the Trefftz method, Petrolito [14,15] presented a hierarchic family of triangular and quadrilateral T-elements for analyzing moderately thick Reissner-Mindlin plates. In these HT formula-tions, the displacement and rotation components of the auxiliary frame field $\tilde{\mathbf{u}} = \{\tilde{w}, \tilde{\psi}_x, \tilde{\psi}_y\}^T$, where ψ_i is defined in eqn (1.76), used to enforce conformity on the internal Trefftz field $\mathbf{u} = \{w, \psi_x, \psi_y\}^T$, are independently interpolated along the element boundary in terms of nodal values. Jirousek *et al*. [11] showed that the performance of the HT thick plate elements could be considerably improved by the application of a linked interpolation whereby the boundary interpolation of the displacement, $\tilde{w}$, is linked through a suitable constraint with that of the tangential rotation component, $\tilde{\psi}_s$. This concept, introduced in [23], has been recently applied by several researchers to develop simple and well-performing thick plate elements [1,5,10,11,22,24,26].

Practical experience with existing HT-elements for thin plates [6] and plane elasticity [9] has clearly shown that, from the point of view of cost and convenience of use, the convergence based on *p*-extension is largely preferable to the more conventional *h*-refinement process [8]. From the discussion in the